Tutor/s

Dr. Josep Puigmartí-Luis
Departament de Ciència de Material i Química Física
Institut de Química Teòrica i Computacional Barcelona (IQTC)

Dra. Maria Guix Noguera
Departament de Ciència de Material i Química Física
Institut de Química Teòrica i Computacional Barcelona (IQTC)

Grau de Química

Treball Final de Grau

Controlled clot formation in microfluidic co-flowing devices.

Formació controlada de coàguls en dispositius microfluídics de coflux.

Marina Luque Artero

January 2023

Universitat de Barcelona

B:KC Barcelona Knowledge Campus
Campus d'Excel·lència Internacional

The intelligence consists not only in the knowledge but also in the skill to apply the knowledge into practice.

Aristotle

En primer lloc, vull agrair als meus tutors, Prof. Josep Puigmartí-Luis i Dra. Maria Guix per haver-me guiat i ajudat durant el desenvolupament del projecte. També vull agrair al grup de recerca ChemInFlow per l'acollida i haver-me fet gaudir del projecte. En especial, a R. Santiago Herrera, pel seu suport, guia i disposició en tot moment.

Per altra banda, agrair a la meva família i amics pel suport i paciència durant aquesta etapa. Principalment, als meus pares que mai han deixat de creure en mi.

REPORT

IDENTIFICATION AND REFLECTION ON THE SUSTAINABLE DEVELOPMENT GOALS (SDG)

In 2015, the United Nations General Assembly (UN-GA) established a series of sustainable development goals (SDG) with the aim of achieving a better and more sustainable future for all. In the 2023 agenda,17 global objectives were settled, which cover various challenges in social, economic, and environmental fields.

The main objective of this project is the development of a microfluidic device that allows generating biomimetic blood clot in lab on a chip device, relying on the natural blood coagulation cascade using whole blood. Through this platform, the activity of anticoagulant drugs could be tested with the aim of reducing stroke deaths, of great interest both for personalized medicine and to reduce the use of animals for research and testing purposes. In this way, this project is addressed to supply goal 3, guarantee a healthy life and promote well-being for all at all ages.

In addition, it has wanted to supply goal 4, guarantee and inclusive, equitable and quality education and promote lifelong learning opportunities for all. For this purpose, the results and images shown in this project rely on the use of color-blind friendly palette. Creating inclusive graphics allows us to bring knowledge closer to those who present color vision deficiencies, reducing the difficulties for bringing knowledge closer.

CONTENTS

1. SUMMARY

A stroke is a medical condition in which brain is poorly supplied by blood flow, causing cell death. There are two types, ischemic when the blood vessel is blocked by the formation of a clot, and haemorrhagic, due to bleeding. Ischemic stroke is the most common type of stroke, accounting for 87% of stroke cases.

The most common treatment consists of the administration of recombinant tissue plasminogen activator (r-tPA) into the bloodstream. However, such treatment approach presents serious side effects such as internal bleeding or swelling. In that regard, ANGIE project is developing an electromagnetic unit that will allow a controlled drug delivery to a desired clot location by using magnetically active robots. The work hereby presented is mainly focused on the design of a microfluidic device to obtain a control blood coagulation, leading to the generation of clots with well-defined rheology and morphology. In a near future, the anticoagulant drugs activity will be tested on the biomimetic clots-in-chip developed in this TFG project, obtaining preliminary results of the magnetic robot's effectiveness in the clot's dissolution process.

Toward that goal, the effect of viscosity and flow was evaluated inside a continuous flow microfluidic device. According to the conducted studies, it was observed that by tunning the flow conditions, the mixing point was changed when using the same channel design. Besides, when working with solutions of similar viscosity to whole blood, a wider distribution profile is observed due to the shear rate effect. Once the system was optimized, clot formation was induced by using $CaCl_2$ solutions with whole blood. Furthermore, from blood coagulation studies, it was determined that there was no correlation between the flow conditions and the morphology of the clots formed by using a simple blood recalcification approach.

Keywords: Ischemic stroke, coagulation, blood, microfluidic system.

2. RESUM

L'ictus és una malaltia en què el cervell està insuficientment alimentat amb flux sanguini, causant la mort cel·lular. N'hi ha dos tipus, l'isquèmic, quan el vas sanguini queda bloquejat per la formació d'un coàgul, i l'hemorràgic, per l'hemorràgia. L'ictus isquèmic és el tipus més comú, i representa al 87% del casos d'ictus.

El tractament més comú consisteix en l'administració d'activador de plasminogen tissular recombinant (r-tPA) al torrent sanguini. Tanmateix, aquest tractament comporta efectes secundaris greus com ara sagnat intern o inflamació. En aquest sentit, el projecte ANGIE està desenvolupant una unitat electromagnètica que permetrà la distribució controlada de fàrmacs a la ubicació desitjada mitjançant l'ús de robots magnèticament actius. Aquest projecte de TFG, se centra principalment en el disseny d'un dispositiu microfluídic que permeti el control de la coagulació de sang, generant coàguls amb reologia i morfologia definides. En un futur, es provarà l'activitat de fàrmacs anticoagulants en coàguls biomimètics en un xip, assolint resultats preliminars de l'eficàcia dels robots magnètics en el procés de dissolució del coàgul.

Amb aquest objectiu, es va realitzar un primer estudi sobre l'efecte de la viscositat i el flux dins del dispositiu microfluídic de flux continu. Segons els estudis realitzats, es va observar que el canvi de les condicions de flux en el sistema microfluídic va provocar un canvi de punt de mescla quan s'utilitzava el mateix disseny de canal. Altrament, quan es treballava amb solucions de viscositat similar a la de la sang sencera, el perfil de distribució dins del canal mostrava un distribució més àmplia degut a l'efecte de la velocitat de cisalla. Un cop optimitzat el sistema, la formació del coàgul es va induir treballant amb solucions de $CaCl_2$ i sang. Així mateix, a partir d'estudis de coagulació de la sang, es va determinar que no hi havia correlació entre les condicions de flux i la morfologia dels coàguls formats mitjançant una aproximació simple de recalcificació de la sang.

Paraules clau: Ictus isquèmic, coagulació, sang, sistema microfluídic.

3. INTRODUCTION

Stroke is the fifth leading cause of death, approximately killing more than 795.000 people per year in the United States.[1] Statistics show that every 3.5 minutes someone dies due to a stroke attack, which occurs when a blood vessel breaks or becomes occluded due to clot formation. When this happens, the oxygen and nutrients supply are cut off to the upstream cells, causing their death. In particular, ischemic strokes are caused by clot formation in the brain vasculature, being the most common one and representing 87% of cases in the world. Moreover, the consequences of an ischemic stroke are catastrophic for the patient, leading to a sudden death or other associated disabilities, such as speech or memory loss, among others.

The obstruction causing an ischemic stroke is defined as clot or thrombi. A clot is based on passive red blood cells that do not participate in the coagulation process and platelets, this last being the responsible of creating fibrin mesh that holds the clot structure. Fibrin is a fibrillar protein that forms three-dimensional networks, and hence, it generates solid structures to stop bleeding.[2] To control the growth and lifetime of a clot, the homeostatic system is completely regulated in biological systems. Besides, clot dissolution is regulated by the activation of specific factors, such as plasminogen. This enzyme catalyses the destruction of the fibrin network into its initial component, fibrinogen.

Currently, the treatment to dissolve clots consists in the injection of tissue plasminogen activator (tPA) through the bloodstream.[3] Alternative treatments are considered at longer time frame conditions, such as mechanical thrombectomy, which is more invasive and require a surgical intervention.[4] The tPA administration causes the plasminogen activation, a serine protease that catalyses the reverse reaction of the fibrin formation. In fact, tPA is an FDA approved drug for the clot dissolution. In an acute patient, tPA is injected in a window of 4.5 h after the first symptom of the stroke attack, and multiple low concentrated doses are required for full recovery.[5] However, some of the side effects of tPA administration are internal bleeding and swelling, among others. In order to reduce such side effects, the ANGIE project aims to develop a magnetoelectric

unit that will allow the controlled delivery tPA in a spatiotemporal manner to any targeted clot location by employing magnetically active robots that will improve clot dissolution by controlled and localised tPA delivery.[6]

In this work, we designed a microfluidic device to study clot formation in a controlled manner to generate a biomimetic clot. With our microfluidic approach, it was possible to control the localization and shape of blood clots, while creating them by exploiting the very same native blood coagulation system. In a near future, such biomimetic clots-in-chip will be later used in the ANGIE project to test the controlled administration of anticoagulant drugs and study the lysis process of morphological controlled clots.

3.1. BLOOD CLOTTING

Blood is a body fluid composed of two phases: plasma, and cellular elements. It presents several functions, such as regulating the body temperature, oxygen and nutrients transport to organs, or clot generation to avoid the blood loss. Plasma is based on a mixture of water (95% by volume), salts, lipids, hormones, and several proteins. It contains inorganic components (Bicarbonate, Fluorine, Iodine, Phosphate Sulphate, Zinc, among others) and organic components (Creatine, citric acid, lactic acid, glucose, fibrinogen as one of the most abundant proteins, among others).[7] The blood cells that play a key role in the coagulation process are,

Erythrocytes (Red Cells): They are passive participants in haemostasis and thrombosis.

Leukocytes (White Cells): They are responsible for generating the blood response to external agents, generating inflammation or scarring. When monocytes (a type of white blood cell and phagocyte) are stimulated they express tissue factor, an integral membrane protein and component of a factor complex enzyme responsible of blood coagulation.[8]

Platelets: They are disc-shaped, non-nucleated cells, whose main function relies on forming platelet plugs during the coagulation process to stop initial bleeding. After their activation, platelets interplay in the coagulation cascade to transform fibrinogen into fibrin.[9]

The coagulation cascade is a biological process where at least 12 enzymatic complexes are involved. Such cascade starts through two different pathways, intrinsic and extrinsic (Figure 1), both converging in a common pathway. The intrinsic pathway is initiated when a rupture of the endothelial wall occurs, leaving the collagen exposed, which leads to platelet adhesion to collagen surfaces after endothelial damage takes place. Collagen is a structural protein that can be found in the endothelial walls of arteries or vessels. When a rupture of the endothelial wall occurs, the collagen is exposed, activating factor XII to factor XIIa in the platelet's surfaces. This factor catalyses the activation of Factor XI, thus initiating the coagulation cascade (Figure 1A).[8,10] On the other hand, the initiator of the extrinsic pathway is the tissue factor (TF), an integral membrane protein. When blood vessels are damaged by a trauma, TF is released from the endothelial walls, forming a complex with factor VIIa that induces the activation of factor X to factor Xa (Figure 1B). This latter does not require the exposition of active surfaces such as collagen, but the activation of platelets to release and activate some of the other coagulation factors.[8,10]

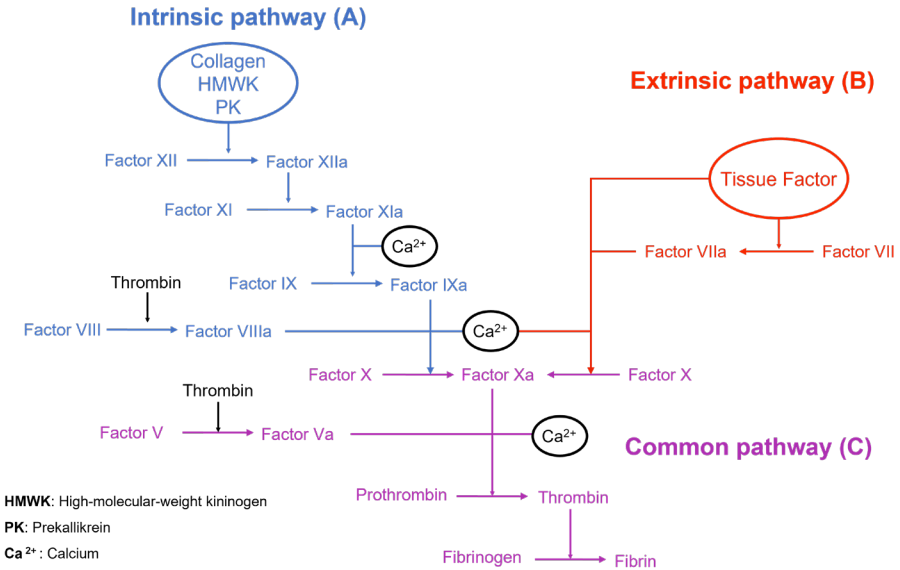

Figure 1. Diagram of blood coagulation by (A) intrinsic pathway; (B) extrinsic pathway and (C) Common pathway.

As it can be seen in Figure 1C, both pathways converge in the activation of factor X. After its activation, the dissolved prothrombin is transformed into thrombin, a serine protease that

transforms the dissolved fibrinogen in the blood into the fibrin mesh of the clot. Although the TF activation paths (extrinsic pathway) seems faster than the collagen-induced one (intrinsic pathway) due to number steps, reaction velocity will depend on the rate constants. Indeed, both pathways end with the formation of fibrin (clot) from fibrinogen, a reaction catalysed by thrombin. When an injury occurs, not only one pathway is activated, but they both work simultaneously. The coagulation cascade is also regulated by calcium, which works as a co-factor in multiple steps, as well as inducing aggregation and morphological shape changes of platelets for their proper activation[11] once the cascade is initiated.

3.2. BLOOD IN MICROFLUIDIC DEVICES

Microfluidic devices allow a fine control of flow rates across microchannels, as well as performing multiple biological tests in parallel depending on the microfluidic channel design. Due to the dimensions of the microfluidic devices, which range from tens to hundreds of micrometres, only a small amount of sample is required to carry out the experiments. Moreover, at the microscale size range, it is possible to obtain materials with new physical properties by controlling mass transport processes, being able not only to tune the reaction kinetics, but also to obtain structures with controlled morphologies (i.e. covalent-organic frameworks).[12] For these reasons, blood coagulation was studied using a microfluidic device.

3.2.1. Reynolds number

In microfluidics, it is key to control the parameters and fluid rheological properties, as well as understanding the undergoing chemical reactions in detail. Fluid dynamics is a well know subfield of fluid mechanics. In the nineteenth century, Claude-Louis Navier and George Gabriel Stokes developed a set of partial differential equations that describe the motion of viscous fluids. In the case of an incompressible Newtonian fluid, with constant density and constant viscosity, the corresponding Navier-Stokes equation is:[13]

$$\rho \frac{\sigma v}{\partial t} + \rho(\vec{v} \cdot \nabla)\vec{v} = \rho\vec{f} - \nabla p + \eta \Delta \vec{v} \quad (1)$$

Where t is the time, $\vec{v}$ is the fluid velocity, ρ the density, $\vec{f}$ the force vector, η the viscosity, and p the pressure. The right side of the equation considers fluid acceleration, thus the velocity of the fluid at each point and its acceleration caused by velocity changes. The left side of the

equation characterizes the forces present in the system, such as external forces, pressure gradients and viscosity changes. The relationship within these forces and accelerations allows to formulate a diverse set of parameters that characterizes the resulting fluid motion, heat, and mass transport, among other phenomenon taking place in the system.

The Reynolds number (Re) is a parameter that determines the relation between the viscous to inertial forces. It allows to describe fluid mobility, thus if a solution flows laminar or turbulent through a channel. Developing such relation from the already described equation (1), allows to formulate Re as (2):

$$Re = \frac{F_{inertial}}{F_{viscous}} = \frac{\rho \cdot v \cdot L}{\eta} \quad (2)$$

Where η is the viscosity of the fluid, ρ the density of fluid, L the characteristic length of the channel and u the linear velocity. In a microfluidic device, the characteristic length values are very small because the channels micrometric dimensions. Therefore, the Re value will be really low and the flow profile described in the channels will be laminar. In this case, the fluid profile does not allow the presence of any turbulence flows. This makes mass transport (i.e., the mixing), to be only controlled by diffusion effects, allowing us to have a fine control over reaction processes. Therefore, at low Re it might be possible to control the mixing point and the position where blood clots will be generated inside the microfluidic device.

3.2.2. Blood viscosity

As we have been previously discussed, at low Re viscous forces predominate to inertial forces. Therefore, when working with viscous solutions, different flow rate profile will be obtained. As per our interest in blood to exploit the natural coagulation cascade to create clots-in-chip, we will look at the rheological properties of blood to make sure that the flow is still laminar. Blood is non-Newtonian fluid with thixotropic properties, i.e., at high shear stresses, it presents lower viscosity values. This is mainly due to blood composition, which is based in two phases: plasma and cellular elements (platelets, erythrocytes, and leukocytes). Blood viscosity will depend on plasma viscosity, haematocrit quantity (the number of erythrocytes), and red blood cell aggregation, among other parameters.[14] According to a study carried out by Shu Dog,[15] at shear rates greater than 10^2 s^{-1}, blood presents a Newtonian behaviour. Therefore, depending on the

applied flow rates conditions, blood profile will be different due red blood cells aggregation at low flow rates (viscosity increases) and deformation at hight flow rates (viscosity decreases).

3.3. OUR SYSTEM

Our system consisted of a chip with 3 inlet ports (two lateral ports and a central port) and 1 outlet (see Figure 2A). The two reagents were added through the lateral inlets, while the solution in the central inlet port allowed the dilution of them two, delaying their mixing point. The cross section of the channel in the chip was 0.5 mm height, 1 mm wide and 13 mm long (Figure 2B). The mixing point was determined by visual inspection using optical microscopy, being able to define the most favourable coagulation conditions and the resulting clot position.

Previously, our device was optimized and a tested with coloured solutions to evaluate the flow rate and viscosity effect in the mixing point along the main channel. Once the device was optimized and the parameters that affect the mixing of the different solution in-channel, the corresponding experiments to study blood coagulation were carried out, inducing clot formation by using $CaCl_2$ solutions. Finally, we studied if there was any correlation between the flow rate and clot morphology.

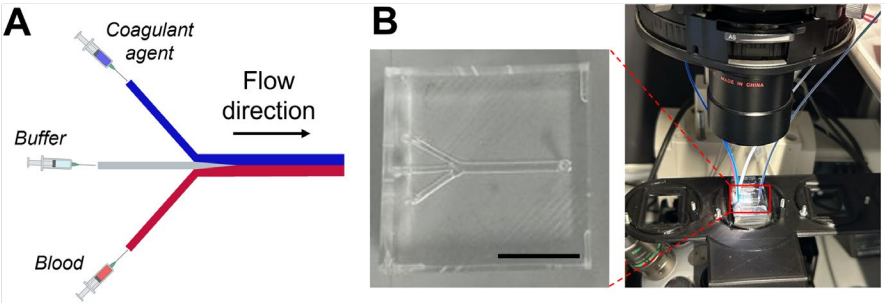

Figure 2. (A) Schematic illustration of the flow configuration in our microfluidic devices; and (B) micrographs of the chip and the microfluidic set-up used in our experiments. Scale bar, 1 cm.

4. OBJECTIVES

The overall goal of this project is the design of a microfluidic device to study the formation of blood clots using in vitro conditions and whole blood to obtain biomimetic structures, both in terms of composition and morphology. To achieve this goal, the next steps were followed:

- Study blood coagulation inside continuous flow microfluidic devices.
- Optimize the continuous flow microfluidic device and determine the variables that will affect the location of the blood clot (e.g., flow rate effect, solution concentration, viscosity).
- Characterize the mesh structure and morphology of the generated blood clots inside the microfluidic devices using confocal microscope.

5. EXPERIMENTAL SECTION

5.1. MATERIALS AND METHODS

Poly(dimethylsiloxane) (PDMS, SYLGARD 184 Silicone Elastomer Curing Agent, DOWN company), DARWIN microfluidic dyes (E E), Mili-Q water, 3,3'-Dihexyloxacarbocyanine Iodide (DiOC6, Sigma-Aldrich), Fibrinogen form human plasma Alexa Fluor 546 Conjugate (Invitrogen), Methylcellulose (Sigma-Aldrich), N-(2-Hydroxyethyl)piperazine-N'-(2-ethanesulfonic acid) (HEPES, Sigma-Aldrich), calcium chloride (Sigma-Aldrich), sodium chloride (Merck), dimethyl sulfoxide (DMSO, Sigma-Aldrich), VAHINÉ food dyes and sodium bicarbonate (Sigma-Aldrich) were all acquired from commercial sources. The mold used was manufactured by The Institute of Bioengineering of Catalonia (IBEC) using a Microlay 3D Printer.

Visual inspection of the lab-on-a-chip systems were done by using a Nikon Eclipse Ti inverted microscope, equipped with a Nikon Plan Fluor 4x 0.13, PhL objective lens and MWWHLP1 Mounted LED to acquire bright field images, and NIKON F66-L000 ET-Triple 400/470-490/550 LED and NIKON TRITC filter to work in fluorescent mode (in both cases the UI-3260CP Rev.2 IDS Camera is used). Viscosity measures were made using a Brooklied Ametek DVE Viscometer and a spindle B-LV-1 (61).

5.2. MICROCHIPS FABRICATION

PDMS is classified as the simplest member of the silicone polymer family and due to its characteristics, being an elastic material, hydrophobic, with poor reactivity and biocompatible, it is perfect for carrying out our experiments with blood.[16] The protocol to manufacture the PDMS-based chips was adapted from Ref. [17]. We performed a standard mold replication process using a rigid polymeric mold. The rigid mold was fabricated using a 3D Microlay printer with a Solus Art Grey V3.0 resin by IBEC. Molds were pre-heated at 80 ºC for at least 30 min before being used. PDMS-based chips were manufactured by replicating the features printed in the molds.[16] A 10:1

mixture of PDMS and SYLGARD 184 (catalyser) was prepared and mixed for 5 min. For each mold used, 44 g of mixture was prepared. Once the bubbles generated during mixing were gone after a deaerated process using a vacuum desiccator, the mixture was poured into the pre-heated mold and left in the oven at 80º degrees for 1 hour. Subsequently, after completing the curing process, we opened holes in the inlet and outlet locations of the device using a SYNEO manual medical hole biopsy puncher to be able to introduce the reagents into the microfluidic chip. Once the PDMS was cured, it was removed from the mold, cut to a specific size (2 x 2 cm) and holes were punched using an N15 catheter puncher SYNEO of internal diameter of 0.072 in and a tube of 0.51 in.

Typically, the chips are attached to glass slides after plasma bond treatment of their surfaces. This process does not allow the extraction of soft-fragile samples produced inside of the chip because the irreversible PDMS bonding to glass requires and strong mechanical forces, and the brittle nature of the glass would perturb sample stability. To solve this limitation, we plasma bonded the chip to a 150 µm thick layer of PDMS. Although the bonding of both layers is also irreversible, PDMS was easy to break without damaging or disturb the sample inside of the chip. Moreover, the injected fluid will not encounter active surfaces that induce blood coagulation.[16] The layer was prepared by a 10:1 mixture of PDMS and catalyser, mixed by 5 min. For each wafer used, 4.4 g of mixture were prepared. Then, the mixture was degasified in vacuum desiccator and poured into the wafer. To coat the wafer, a WS-650-23 spin coater was used at 500 rpm pending 60 seconds after spreading the mixture for 10 s at 500 rpms. Next, the wafer was left for 15 min on a flat area to ensure that PDMS evenly covers the wafer. Afterwards, the wafer was left on a hot plate at 125ºC for 5 min to cure.

The PDMS chips and PDMS thin layer were coupled by plasma bonding in a Plasma Cleaner (PDC-002-CE, Harrick Plasma). During this process, organic hydrocarbon material was chemically removed with highly reactive oxygen radicals using plasma at 0.6 mmHg pending 90 seconds. In this way, PDMS surfaces were activated by silanol (SiOH) groups. When both surfaces got into contact with each another, a Si-O-Si bridging bond was formed, creating an irreversible seal. Then, the final device was cured for 1.5 h at 120 ºC before its use in the experiment.

5.3. PREPARATION OF SOLUTIONS

5.3.1. Test dye Colors

To evaluate the effect of the flow rate at the mixing point, two red and blue solutions were prepared with DARWIN microfluidic dyes. E129 dye solution consists primarily of Allura Red, a red disodium salt, and an azo-derived compound.[18] On the other hand, the E133 sky blue solution is mainly composed of brilliant blue FCP, a blue coloured sodium salt.[19] Both the E133 sky dye and the E129 red dye are mainly based by sodium salts and no-side reaction in-chip will take place, allowing the study of diffusion and mixing processes. These reagents allowed us to study the colour change along the microfluidic channel and identify the key parameters for in-chip clot generation. The solutions were prepared at the following concentrations:

Red solution preparation: To prepare a 10% solution in a 10 mL vial, we took 500 µL of E129 red dye and added in 4.5 mL of Mili-Q water.

Blue solution preparation: To prepare a 10% solution in a 10 mL vial, 500 µL of E133 blue sky dye was added in 4.5 mL of Mili-Q water.

The solutions were properly stirred to ensure the complete pigments dissolution. These dye concentrations were used because they allowed correct color change visualization along the channel.

5.3.2. Test viscosity with dyes colors

To observe the effect of viscosity on the mixing point, methylcellulose solutions were prepared at different concentrations. Methylcellulose (MC) is a derivate of cellulose that presents amphiphilic properties that characterize its rheological properties. These properties are a function of the MC concentration, temperature, and shear rate. At low temperatures (below 30 ºC) MC concentrated solutions typically show a Newtonian behaviour, i.e., the viscosity of the fluid is dependent on the concentration and the degree of polymerization of the MC chain. At temperatures above 30ºC the behaviour of MC solutions is non-Newtonian and the viscosity of the fluid becomes strongly dependent of the shear rate, even at very diluted concentrations.[20] Our experiments were performed at room temperature, thus MC solutions at a determined concentration and degree of polymerization are suitable for modeling the blood flow. In this way,

MC solutions were prepared at low temperatures (2-8 ºC) to maximize its solubility, and the experiments were later performed at temperatures between 20-25 ºC. We did not observe MC precipitation at the working conditions. Besides, we measured the bulk viscosity of the MC solutions using a DVE Digital Viscometer (Ametek Brookfield) with a spindle B-LV-1 (61). The viscosity measurement was kept at the same share rate to obtain comparable results.

Methylcellulose solutions preparation (Red flow): To a 25 mL vial, methylcellulose (0.1 g) was added to Mili-Q water (20 mL) **(solution A**). To a 25 mL vial, methylcellulose (0.2 g) was added to Mili-Q water (20 mL) (**solution B**). Methylcellulose is insoluble in hot water, but at low temperatures (5 ºC) it presents greater solubility in water.[20] Afterwards, solutions were left in the refrigerator for 24h at 2-8 ºC to reach a complete solubilization.

To a 25 mL vial, methylcellulose solution (A, 4 mL) was added to Mili-Q water (16 mL) to obtain a 0.1% solution. To a 25 mL vial, methylcellulose solution (A, 2 mL) was added to Mili-Q water (18 mL) to obtain a 0.05% solution. To a 25 mL vial, methylcellulose solution (A, 0.4 mL) was added to Mili-Q water (19.6 mL) to obtain a 0.01% solution. To a 25 mL vial, methylcellulose solution A (10 mL) was added to Mili-Q water (10 mL) to obtain a 0.25% solution.

To carry out the viscosity change experiments, 0.25% and 1% (**B**) solutions were used, being the solutions with higher viscosity. To a 25 mL vial, E129 red dye (0.5 mL) was added to solution at 0.25% (4.5 mL). To a 25 mL vial, E129 red dye (0.5 mL) was added to solution at 1% (4.5 mL).

Blue solution preparation: To prepare a 10% solution in a 10 ml vial, 500 µL of E133 blue sky dye was added in 4.5 ml of Mili-Q water.

5.3.3. Test blood

To carry out the experiments with blood, sheep blood samples were supplied by Vall d'Hebron Barcelona Hospital. Blood was extracted in 6 mL vacutainer tube (BD Vacutainer) containing citric acid as anticoagulant and dextrose to increase the viability of the blood components (trisodium citrate, 13.2 g/L; citric acid, 4.8 g/L and dextrose 14.7 g/L). The protocol is described in more detail in the following paragraph. Blood was safety transport at low temperatures (2-8 ºC) and consequently stored in refrigerator before its use. Platelets were stained with a fluorescent chromophore to visualize their movement along the channel, since they play a key role in the coagulation cascade. Moreover, platelet aggregation in the fibrin mesh will help us to track and

properly identify clot formation in chip. Stained fibrinogen was also added, so that when fibrin was formed from fibrinogen, the generated clot was clearly visualized by fluorescence.

Blood sample preparation: Fluorescent dyes solutions were previously prepared by following the blood sample preparation protocol developed in the laboratory. The staining solutions were stored in small Eppendorf's at -20 ºC before their used. It was prepared a 1 mM solution of $DiOC_6$ in DMSO for fluorescently labelling the platelets. Fibrinogen form human plasma Alexa Fluor 546 Conjugate was prepared as recommended by the manufacturer. A 5 mg sample was dissolved in 0.1 M sodium bicarbonate solution at pH 8.3 to obtain a final chromophore concentration of 3.3 mg/mL (aliquots of 20 µL were prepared and stored in the refrigerator). In the following experiments, samples were left to thaw at room temperature before use. Blood sample was allowed to reach room temperature as well before its use. 1 mL of blood was withdrawn from the tube using a 1 mL B BRAUN syringe and a sterile STERICAN hypodermic needle, both placed in a small Eppendorf. DiOC6 solution (5 µL) was added to the blood sample and shaken carefully to get a final concentration, obtaining a final concentration of 50 µM DiOC6 in the blood sample. Then, it was left in the water bath at 37ºC for 5 min. Afterwards, 50 µL of blood were withdrawn and added to 20 µL of the stained fibrinogen. We withdrew and returned this latter to the same initial Eppendorf and repeated the process 3 times to make sure that marked fibrinogen was correctly added to the main sample. With this, we reached a final concentration of 0.19 µM of stained fibrinogen. The mixture was gently shaken to be fully homogenized and left in the water bath until the experiment started.

Buffer preparation: To a 25 mL vial, NaCl (0.09 g) was added to Mili-Q water (10 mL). Then, the solution was stirred until homogenize. Then, an HEPES solution (1 M, 10 µL) was added to the solution and stirred. HEPES is a buffer at pH 6.8 to 8.2 used for blood sample stabilization.[21] If the pH is less than 7.35 the blood will become acidic, and if its pH becomes higher than 7.45 it is too basic for blood stability. So, to maintain the normal conditions in blood (7.35-7.45 pH) HEPES solution was required.[22]

$CaCl_2$ solutions preparation: To a 10 mL vial, Blue brilliant FCF (0.05 g) was added to Mili-Q water (5 mL) and was stirred until homogenize to obtain the blue dye solution. To a 15 mL vial, blue dye solution (1 mL) was added to Mili-Q water (10 mL) and then stirred to obtain the control

solution. To a 15 mL vial, $CaCl_2$ (1.1 g) was added to Mili-Q water (9 mL) and blue dye solution (1 mL), stirring them till homogenize to prepare a 1 M $CaCl_2$ solution.

5.4. DATA COLLECTION

Once solutions were prepared, all syringes were fully filled to proceed with the experiment. At all cases, air bubbles must be avoided in the syringes, as it would cause alterations that would later affect the flow rate of the solution, leading to non-reliable results.

Different syringes were used depending on the experiment:

Test dye colours: 5 mL B BRAUN syringes were used for the lateral solutions (red and blue solution) and a 10 mL B BRAUN syringe for the central solution (Mili-Q).

Test viscosity with dye colours: 5 mL B BRAUN syringes were used for the lateral solutions (methylcellulose solutions and blue solution) and a 10 mL B BRAUN syringe for the central solution (Mili-Q).

Test blood: 3 mL B BRAUN syringes were used for the lateral solutions (Blood sample and $CaCl_2$ solutions) and a 5 mL B BRAUN syringe for the central solution (Buffer solution).

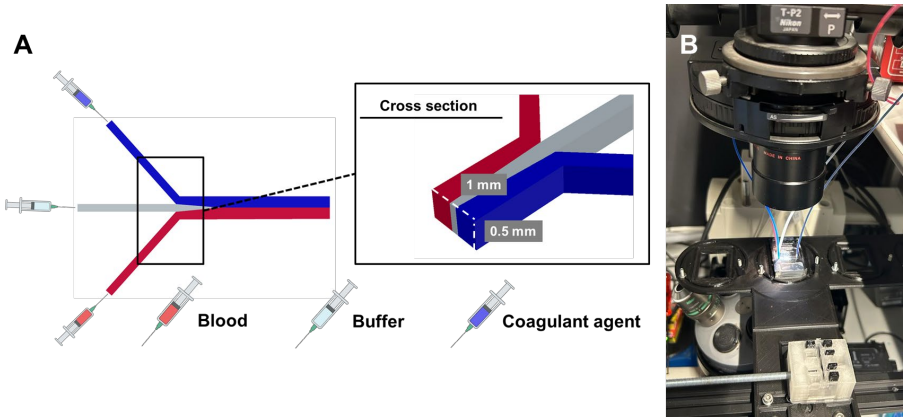

Figure 3. Pictures of (A) schematic of microfluidic injection; (B) microfluidic system

First, the chip was placed in a homemade adaptor in the microscope aimed for advanced image acquisition of all the sections of interest along the channel. Next, the syringes were placed in the injection system (Nemesys syringe pump, Cetoni). To connect the syringes to the chip

inputs, 4 polytetrafluoroethylene tubes (Vici Vour) with a 0.5 mm inner diameter were cut and placed in each syringe. In this step, it was key to not introduce air through the channel when connecting the tubes to the inlets. To avoid this, the buffer solution was circulated through the central inlet. Once the solution was observed to be coming out of all the three inlets, the other tubes were plugged in. The flows were place as in Figure 3A. The injection system was operated at the different flow rates studied. We used a homemade automated image acquisition system previously developed in the laboratory to systematically obtain the images of the chip channel (see Figure 3B), which were taken at a frame rate of 77 fps. The system allowed us to move along the channel and acquire an image of each section, only requiring 4 images to completely reconstruct the whole channel length. We considered an overlapping larger than the 10 % of the image size to facilitate the final image reconstruction. Each acquired image had an initial size of 1936 x 1216 px, leading to an expected theoretical size of 6969 x 1216 px after joining the 4 images. Because of the reconstruction with the ShotCut and the zoom out of 22%, the final reconstructed image size decays to 1140x218 px. However, this resolution loss with respect to those taken from each section did not affect the analysis neither the final obtained results.

5.5. DATA TREATMENT

Once the images were acquired as described in 5.4. section, in order to obtain a final image of the entire channel, we followed the protocol detailed in appendix 1. This processed image is then analysed using a homemade code in MATLAB to determine the mixing point (F_{mix}) along the channel. Firstly, the code was loaded and the image of the channel uploaded (Figure 4A), indicating in the code the scale in mm/pixels (different for each group of images) and the frame rate. When the corresponding masks were loaded, the region of interest of the channel was selected (Figure 4B). The colour tones between white and black (grayscale) can be transcribed into numerical values, being possible to correlate the colour change to the mixing values. The numerical range used was from 0 to 255, which corresponded to the colour tones from black to white, i.e., gray scale.

As the code was read in Matlab, the loaded images were separated into different colour channels:

Red channel: Anything red and white will be showed as white.

Blue channel: Anything blue and white will be showed as white.

Green channel: Will display the red and blue channel overlap.

Afterwards, the channels were overlapped, displaying the values of the blue channel in the red one (Figure 4C). To increase the contrast of the images, the values of the red channel were subtracted from values of the green channel. In this way, anything presenting a colour that was not red, was marked black since it presented values of 0. The procedure was applied to increase the blue channel contrast (Figure 4D). Finally, the values of the two images in which contrast was increased, were subtracted. A final image was generated showing everything with 0 value in black, showing everything that is not red or blue will be depicted in white. Therefore, following this image processing protocol, it was possible to easily determine that when both dyes were mixed (Figure 4E). The Matlab script also provided a graph where the mixing percentage of the two solutions was represented, as well as their sum with respect the position along the channel (Figure 4F). Therefore, if a mixing value of 100 % was reached, the solutions were assumed to be mixing. The values were saved in an Excel for further analysis.

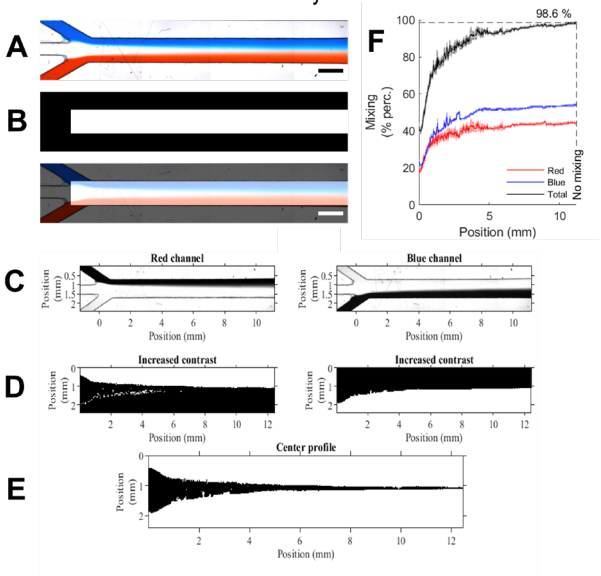

Figure 4. Pictures of (A) Colour image of the channel at 5/20/5 flow rate. Scale bar, 1 mm; (B) Image channel with BB mask. Scale bar 1 mm; (C) red and blue channel inverted; (D) images of red and blue channel inverted and increased contrast; (E) centre profile; (F) F_{mix} along the channel position.

6. RESULTS AND DISCUSSION

6.1. CONTROL OF MIXING POINT

Preliminary tests were carried out to optimize and evaluate the system robustness. Afterwards, a study of the effect of changing de flow rate and viscosity was performed to elucidate the variables that affect the system in order to later proceed with the blood tests.

6.1.1. Optimization of the microfluidic system

Studies on the flow rate effect were carried out with chips fabricated from a rigid mold made with a R19 3D printer (BCN3D). The main problem they presented was that, although the lateral solutions had the same lateral flow condition and were the same fluid (water), they did not present the same profile (Figure 5A). Therefore, it was clear that there was a problem in the geometry of the chip channel and such chips were not reliable, as the profiles were not. Since there was really no control of F_{mix} if the lateral flows do not present the same profile, these chips were discarded, and a new mold was fabricated. The solutions used on the discarded chip were prepared in the same way, but instead of VAHINÉ food dyes, we used DARWIN microfluidic dyes. In figure 5B, the red channels images of the two chips are shown. As previously discussed, red channel showed everything that was not red and white as black. According to the spectrum absorption of Brillian Blue FCF[23] and Amaranth Red Dye,[24] red solution will only be shown as red. From these images we can extract that the red solution of the discarded chip is not purely "red" (Vahiné dye), as the colours cannot be correctly differentiated (Figure 5B). So, as the data treatment was based on the solutions pigmentation, they were discarded. As can be seen in Figure 5, the lateral flows of the chips manufactured from the new mold presented identical profiles, so the studies carried out with them can be taken as valid. All results shown in this report were performed with the optimized chip and Darwing microfluidic dyes.

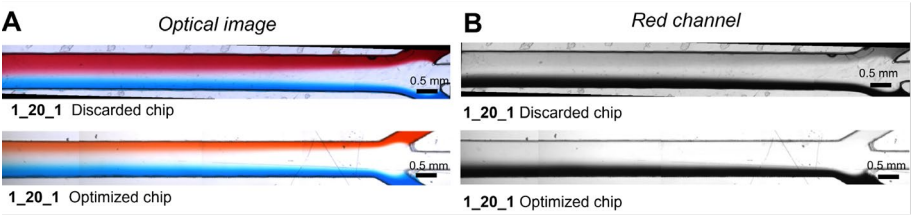

Figure 5. Pictures of (A) Optical image at 1/20/1 with discarded and optimized chip; (B) Red channel image at 1/20/1 with discarded and optimized chip.

6.1.2. Flow rate effect

The effect of the flow rate on the mixing point was studied by using coloured solutions (red and blue). The following flows were evaluated, obtaining the following values (Table 1):

Initial channel schematic	Central flow rate (µL/min)	Lateral flow rate (µL/min)	Lateral flow rate ratio (LFRR)	Central flow rate ratio (CFRR)
	60	1	0.016	0.968
	40	1	0.024	0.952
	60	5	0.071	0.857
	20	1	0.045	0.909
	40	5	0.100	0.800
	60	10	0.125	0.750
	20	5	0.167	0.667
	40	10	0.167	0.667
	20	10	0.250	0.500

Table 1. Summary of channel flow rates and the corresponding schematic of the coloured solutions at the beginning of the main microfluidic channel depending on the experimental conditions applied.

These chosen flow rates allowed us to evaluate the effect of changing the flow conditions and to determine if the solutions presented a laminar flow profile. As explained above, the Re provides information about the behaviour of the liquid flow profile in our system. This depends on the viscosity and density of solutions, as well as the characteristic length, which was set 0.5 mm. The channel parameters used to calculate Re are shown in table 2:

Channel parameters	
Width (mm)	1
Height (mm)	0.5
Cross section (mm^2)	0.5

Table 2. Schematic and corresponding microchannel dimensions.

Parameter	Water	Blood
Viscosity (cP)	1.31	3.50
Viscosity (kg/m*s)	0.131	0.35
Density (kg/m^3)	999.97	1060

(a) The water viscosity was measured using a Brookfield Ametek DVE Viscometer

(b) The blood viscosity value is used assuming that the behaviour of the blood will be Newtonian under working conditions.

Table 3. Viscosity and Density parameters. The density value from blood was extracted from ref. 14, while the density value was obtained from ref. 28.

Table 2 depicts a diagram showing the chip channel dimensions. The cross section and the flow area was calculated by multiplying the width by the height. The characteristic length is a dimension used to define the scale of a physical system, being generally stablished as the smallest feature in the system. Therefore, we considered the height of the device as the characteristic length. By dividing the flow rate (m^3/s) with the cross section (m^2), the linear velocity was calculated.

To obtain the shear stress rate we assumed that the flow rate was related to the channel geometry, considering a constant pressure in the microchip channel. Then, the shear rate (s^{-1}) was calculated by dividing the linear speed (m/s) by the characteristic length (m). Further experiments are required to determine if this approximation is correct. Finally, the Re was calculated using eq.2, obtaining also the values of density and viscosity per each solution (table 3). The final values of Re are shown in Appendix 2. In Figure 6 we evaluated the effect that flow

rate and viscosity have on flow behaviour. Firstly, the obtained Re increase as the shear rate and total flow rate increased. Also, as Re values were small under experimental conditions used, the flow should be considered laminar. We can also extract from the graph that the Re tends to increase more when the solution is less viscous (consider that blood and water present a similar density value).

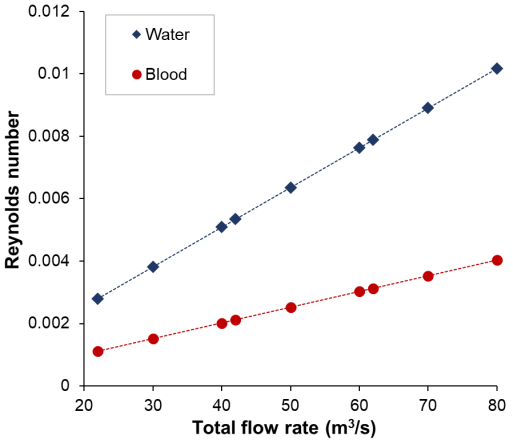

Figure 6. Reynolds number (Re) evaluation. Study of the Re at different flow rates for water and blood samples.

Once we had determined that solutions behaviour was laminar, the corresponding experiments per each flow rate were performed. To evaluate the system reproducibility, the obtained F_{mix} values were plotted against the channel position, considering different days and the same flow rate (Figure 7A). As it can be seen, the F_{mix} values were similar between the experiments, highlighting the stability of the devices and reproducibility of the experiments hereby performed. By representing the F_{mix} values against the position of the channel (Figure 7B), we observed that the lateral flow rate ratio (LFRR) increased, as well as the F_{mix} values, along the length of the channel. However, the results obtained at 0.045 LFRR present a similar behaviour at 0.1 LFRR. This latter effect could be due to not properly plugging the inlets or the presence of air bubbles in the microfluidic device.

It is also important to point out that there was a relation between LFRR and the F_{mix}. To further study such effect on the LFRR, the F_{mix} values obtained at 6 mm position (approximately the

middle of the channel) were plotted with respect to LFRR. In Figure 7C, we can conclude that F_{mix} increases with the LFRR.

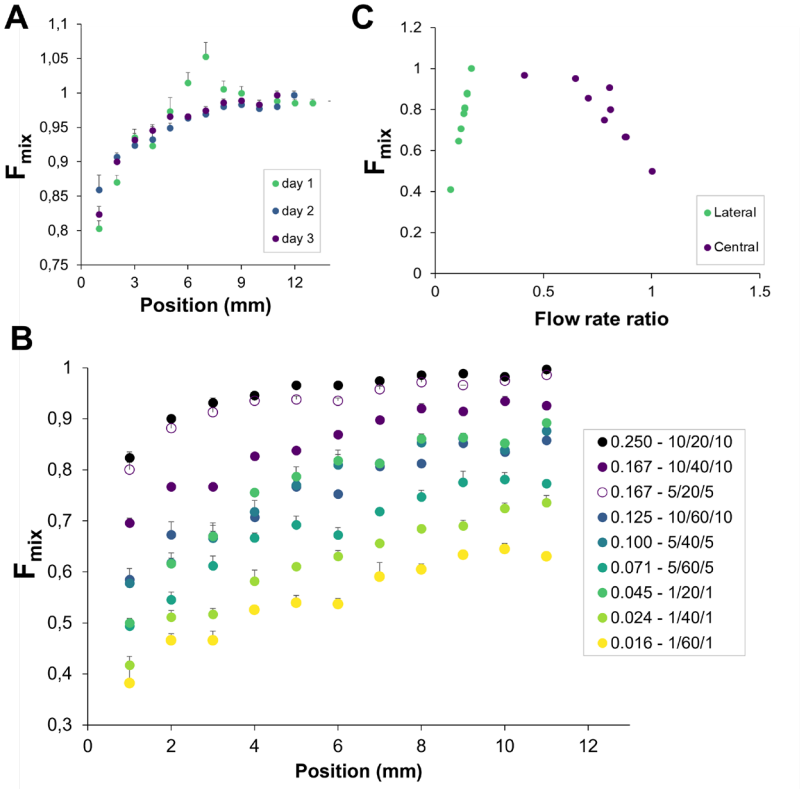

Figure 7. F_{mix} evaluation. (A) F_{mix} values along the channel position by working at 10/20/10 flow rates at different days; (B) Effect of flow rates in F_{mix} at 6 mm position along the channel; (C) F_{mix} values along the channel position at different flow rates in a same day.

A study of the effect of central flow rate ratio (CFRR) was also carried out (Figure 7C). As the CFRR increased, the F_{mix} decreased. This was because the central solution diluted the lateral solutions, so the point at which lateral solutions mixed (mixing point) was delayed. Therefore, the control of flow condition allowed to set the mixing point at different locations in the microfluidic device. Also, for the same channel section, F_{mix} will increase if LFRR increases and CFRR decreases.

6.1.3. Viscosity effect

A study of the effect of viscosity on the mixing point was carried out to better understand how blood will behave in our device, as it is categorized as a non-Newtonian fluid. To do so, we worked with the same flow rates described in the previous section, using methylcellulose (MC) solution as a model Newtonian fluid at room temperature. To tune its viscosity, we worked at different MC concentrations. Because of its rheological properties, the viscosity will remain constant at any shear stress applied.

The viscosity of different methylcellulose solutions was evaluated at different speed (results shown in Appendix 3). The values chosen speeds were at 50 and 100 rpm, as at lower speeds the viscosity values obtained were out of range. Besides, it was not possible to determine the viscosity of methylcellulose solutions at concentrations higher than 0.25% (another needle would be required).

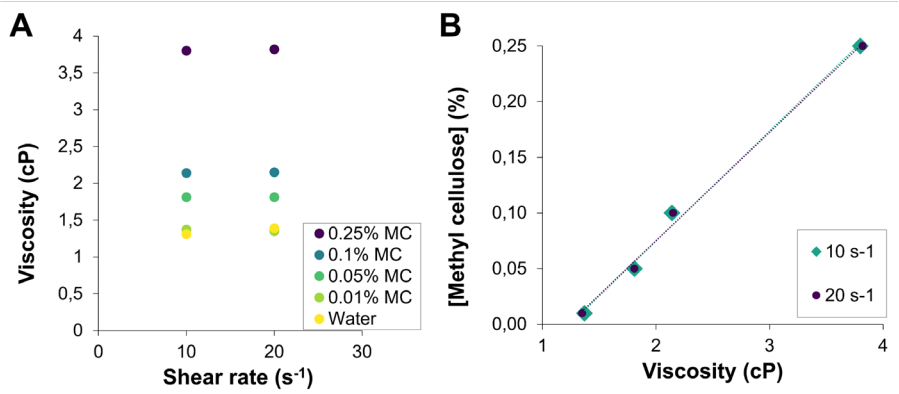

Figure 8. Plots of (A) Viscosity against shear rate; (B) Methylcellulose concentration solutions against viscosity at different shear rate.

The values at 50 and 100 rpm were plotted to verify that the methylcellulose solutions indeed presented a Newtonian behaviour (Figure 8A). The obtained results showed that the values obtained at 50 and 100 rpm can be considered practically identical. Since the tested MC solutions present the same concentration and they have a similar viscosity value at the different studied

shear rates, we can consider MC solutions exhibit Newtonian behaviour. Moreover, we observed that viscosity increased with methylcellulose solution concentration of (Figure 8B).

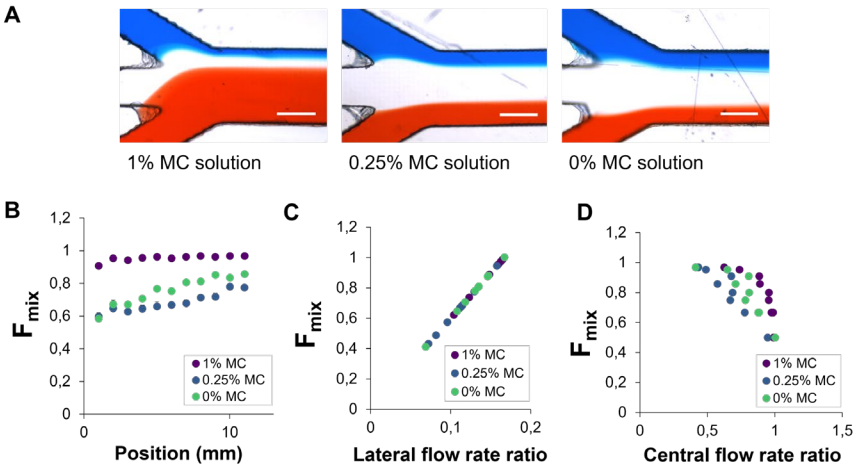

Figure 9. Optical images of (A) Fluid profiles at the beginning of the channel at different MC concentrations and 10/60/10 flow conditions. Scale bar, 0.5 mm; (B) F_{mix} representation against channel position (mm) at different MC concentrations and 10/60/10 flow condition; (C) Representation of F_{mix} against lateral flow rate ratio at different MC concentrations; (D) F_{mix} representation against central flow rate ratio at different MC concentrations.

As shown in table 3, blood presents a viscosity of 3.5 cP measured at high shear rates. Therefore, we worked with 0.25% solutions, which present a viscosity of 3.80 cP, similar to blood's viscosity in the human body.[14] In addition, to evaluate the effect of highly viscous solutions inside the chip we worked with a 1 % solution, as blood shows a thixotropic and behaves as shear thinning fluid. In figure 9A, we evaluated the effect of viscosity on the fluid profile. As the viscosity of the red dye solution increased, its width portion in the channel also increased. However, at a concentration of 0.25 % methylcellulose (3.8 cP), hardly any changes in the solution profile were observed with respect to the 0 % methylcellulose solution. Therefore, the width of the solution in the channel was affected by the viscosity.

To assess whether F_{mix} is affected by the solution profile, the F_{mix} values were plotted against the channel position at different methylcellulose concentration (Figure 9B). As we can see, as the viscosity increased, F_{mix} decreased along the channel. In addition, a study of the effect of LFRR

on the F_{mix} along the channel while evaluating different MC concentrations was carried out (Figure 9C). We can observe that the F_{mix} increased linearly with the LFRR, even working with solutions with different viscosity values. Moreover, the effect CFRR F_{mix} along the channel was also studied (Figured 9D). As the central flow increased, the F_{mix} decreased along the channel. The F_{mix} behaviour in response to changes in flow condition was similar to what was observed in the previous experiments.

To conclude, the viscosity of the solutions influences the F_{mix} values along the channel. As the viscosity of lateral solutions and the LFRR increased, the F_{mix} increased at the beginning of the channel. We observed that, independently of the viscosity, the system properties, such as the control of mass transport by diffusion, should be considered the same. Therefore, viscosity change will only change the F_{mix} at a given flow rate condition.

6.2. COAGULATION CONTROL

To characterize our system as a valid model for clinical studies, we evaluate its reproducibility and robustness by doing several blood tests at different coagulation conditions using calcium chloride ($CaCl_2$) as a coagulant agent. The first one was the control, where 0 M $CaCl_2$ was used, observing no clot formation. In fact, this experiment also validated that there was no coagulation when anticoagulated blood was in contact with PDMS, which could act as an active surface. When blood encounters an artificial surface, proteins are adsorbed based on their diffusion. Then, the non-activated platelets detect the adsorbed protein layer as abnormal, and they become adhere to the adsorbed layer. In this way, platelet activation is initiated, and the coagulation cascade is activated.[9] However, PDMS demonstrated to be a compatible material, as no coagulation occurs if the blood is not recalcified.

To induce clot formation, 1 M $CaCl_2$ solution was co-flowed with the blood. Due to the geometry of the chips used in the initial TFG period, as explained in section 6.1.1., the results were not valid and therefore most of the obtained results were rejected (Appendix 4). For this reason, the results shown with blood were carried out with just one replica (n=1). To determine how long it takes for blood to clot in our system, with the optimize chips, several tests were performed at 1 M $CaCl_2$ at different flow rates. The obtained results established that clot formation could be observed within 20 min for most of the studied flow rates. If we went over 20 min

coagulation time, the clot generation was not localized, neither its shape or size, leading to an uncontrolled clogging along all the microchip channel and even in the tubing system.

As previously mentioned in section 3.1., during the coagulation cascade fibrinogen is converted to fibrin, a reaction catalysed by the thrombin enzyme. From the platelets, after their activation and blood recalcification, the fibrin mesh is formed, with adhered active platelets that continue catalysing the reactions in coagulation cascade. Therefore, to properly follow the coagulation process in our system, fibrinogen and platelets in blood were labelled using fluorochromes (DiOC6[25] and Alexa Fluor 546[26]) that allowed the clear visualization of the clot formation. According to the corresponding fluorochromes emission spectrum, platelets were stained green, while fibrinogen was stained yellow.

We observed that no clot formation was taking place in absence of $CaCl_2$ (see Appendix 5). We did not visualize aggregations of platelets, neither the presences of a fibrin structure after 20 min of reaction. Figure 10A depicts the fluorescence images of the channel at different flow rates after 20 min with the co-flow of whole blood and a 1 M $CaCl_2$ solution. After 5 min, practically no clot formation was observed in any of the studied conditions. However, after 10 min, just for the 5/40/5 flow rate condition, the clot formation was observed at the end of the channel. Finally, after 20 min, coagulation was taking place for all flow rates, except from 1/60/1 flow rate condition.

To better visualize the clot generation, in Figure 10B we only highlighted the stained fibrinogen and the produced fibrin structure. The clot shape seems to differ, as at 1/20/1 and 1/40/1 the clot formed was not as laminar than at 5/20/5 and 5/40/5 flow rates conditions. This can be a consequence of the low shear rate experienced by the blood flowing at 1 µL/min. Therefore, by working at a higher lateral flow rate, the coagulation presents a more linear appearance.

In figure 11A, the effect of LFRR on channel position has been plotted. As the LFRR increased, the position of the channel in which coagulation begins was lower. On the other hand, if CFRR decreased, coagulation started at a position closer to the inlet's junction (see Figure 11B). In this case, the calcium ions must diffuse through the interface. The longer the reagents were in contact, the highest the concentration of calcium ions diffused towards the blood. This latter effect depends in the CFRR, and changes in the flow rate of the central inlet will lead to different contact times.

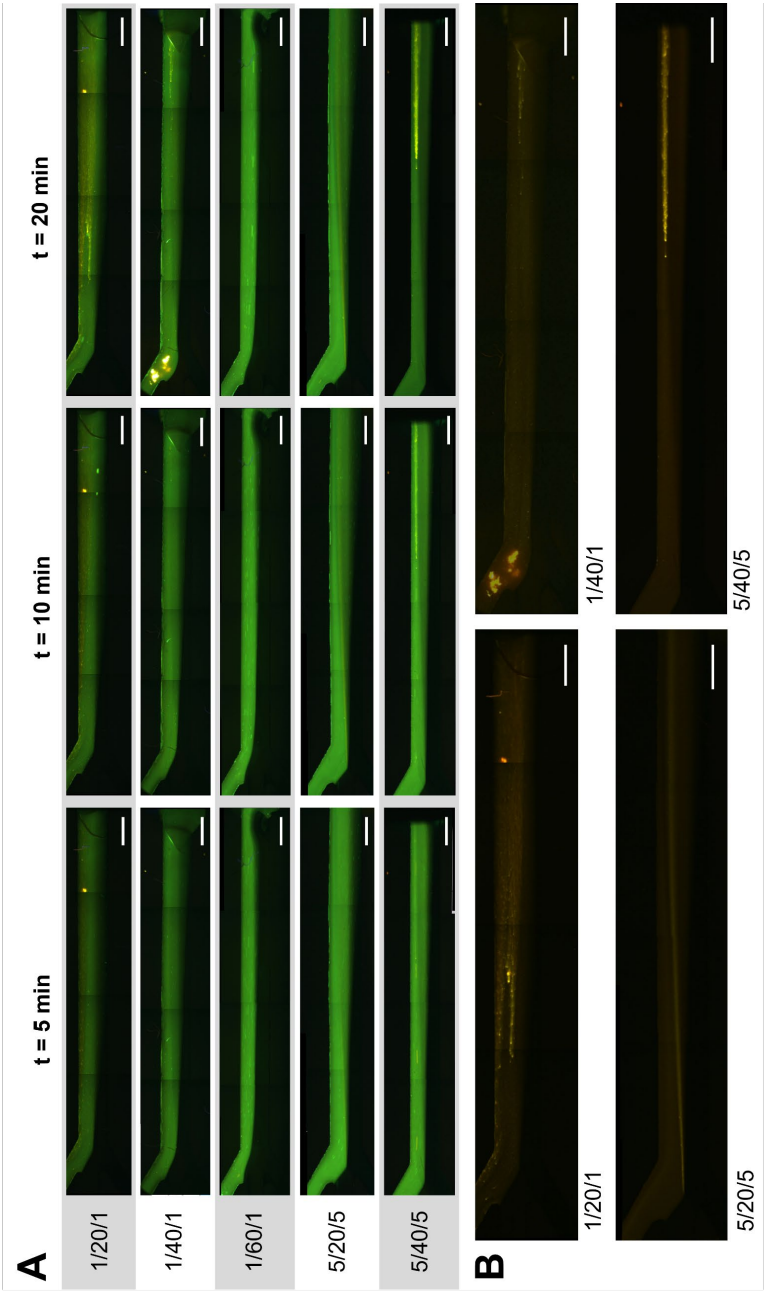

Figure 10. Fluorescent images were taken using a (A) NIKON F66-L000 ET-Triple 400/470-490/550 LED; (B) NIKON TRITC Filter Cube Set. Scale bar, 1 mm.

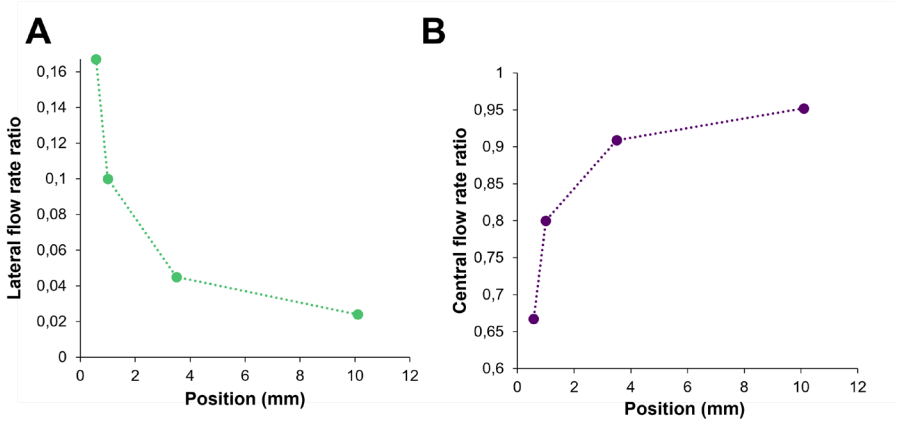

Figure 11. Plots of (A) Lateral flow rate ratio effect on the initial point of coagulation along the channel; (B) Central flow rate ratio effect on the initial point of coagulation along the channel.

Finally, a comparative study considering the effect of the initial solutions profile was carried out. In fact, we observed that the blood profile did not correspond to the one obtained with 0.25% MC solution (3.8 cP) (Figure 12). The width profile of the blood solution inside the chip increased as lateral flow increased, and central flow decreased. When comparing the blood flow profiles with MC solutions, the profiles obtained at high concentrations were similar. Therefore, under the applied experimental conditions, blood did not behave as a solution of a 3.8 cP viscosity value, as initially expected. Therefore, due to the low shear rate (comparable to MC solutions larger than 0.25 %) we assumed that blood presents a large viscosity value. Indeed, we observed that blood did not have a constant viscosity in our device, and it depended on the shear rate at which we worked. Nevertheless, these experiments demonstrated that the blood still presented a laminar blood profile, as well as the expected properties at low Re times. Therefore, the imposed flow rates will determine the coagulation point and thus, the location of the generated clot.

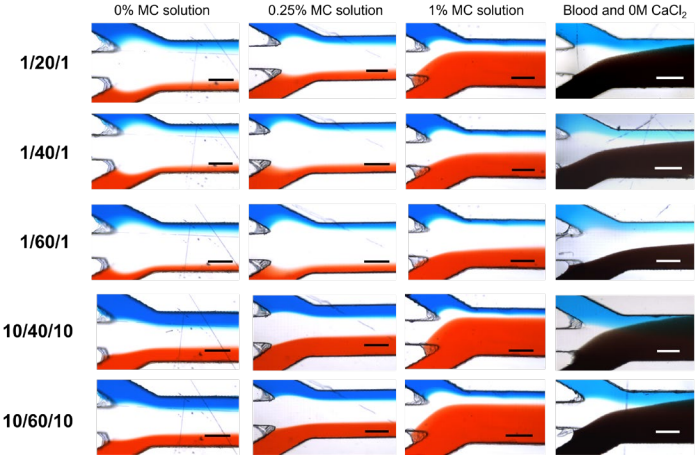

Figure 12. Initial flow profiles at different flow conditions. Scale bar, 0.5 mm.

Furthermore, the mixing point, did not correspond to the initial coagulation position (Figure 13). As the blood was anticoagulated with a citrate salt, calcium ions in the initial blood were chelate. To stop the coagulation process, an excess of the anticoagulant must be added, otherwise free calcium ions or deposits in the blood entities can induce non-controlled coagulation. In our case, a constant flux of calcium is delivered to the blood when both solutions get in contact. In fact, it is important to note that blood coagulation will not take place until the excess of chelate agent is overcome. As a consequence, the contact point of the two fluids and the initiation of the clot did not share the same location. However, other factors will play a key

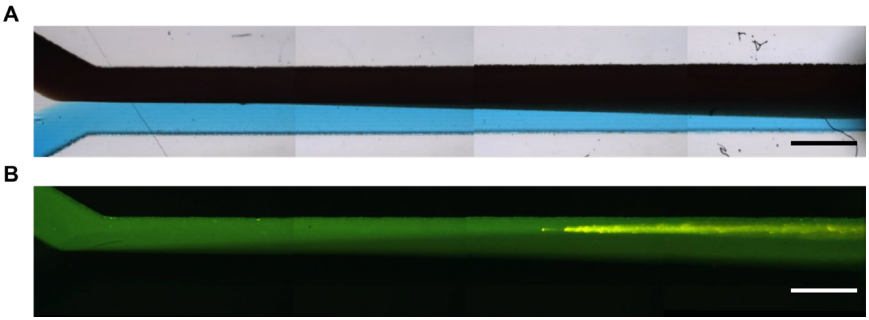

Figure 13. Images at 5/40/5 flow condition using (A) Bright-Field microscopy; (B) Fluorescence microscopy. Scale bar, 1 mm.

role, like the flux of ions that depends only in the diffusion coefficient, and the time it takes to the platelets to get activated after the blood recalcification.

6.3. CLOTS CHARACTERIZATION

To assess whether the flow rates caused changes in the shape, size and the mesh structure of the clot, fluorescent confocal microscopy characterization was performed. In figure 14, we observed fibrin fibers stained with Alexa Fluor 546 in the clot structure, shown in red. This latter is a fake color, defined during the data acquisition in the confocal microscope experiments.

After the clot characterization we can conclude that the fibrin fibers remain parallel to channel, regardless of flow condition. In fact, there was not much difference between the orientation and internal structure of the clots when working at different flow rates. Therefore, we could say that there was no effect of flow rate on the final clot structural characteristics. However, it will be necessary to perform more replicates to extract valid conclusions regarding the different parameters discussed in section 6.2 and how they impact on the final clot shape and morphology.

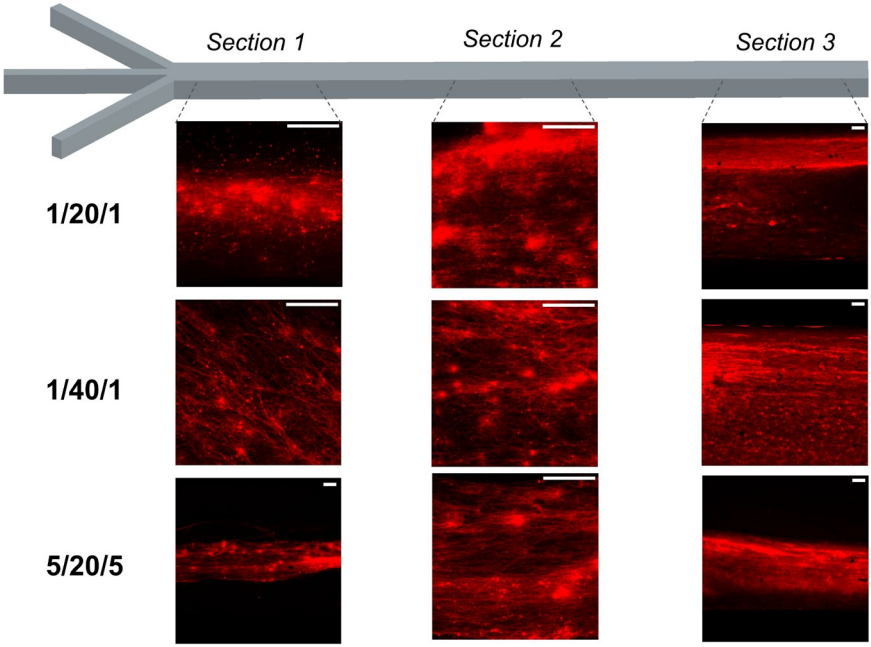

Figure 14. Confocal images of clots generated at different flow rates as explained in section 5.4. Scale bar, 1 mm.

7. CONCLUSIONS

In conclusion, in the current TFG project we have:

- Designed and optimized a microfluidic system for the controlled generation of biomimetic clots in chip by direct blood coagulation. Also, it was demonstrated that the system was robust and reproducible.
- Demonstrated the effect of changing the flow rate on the mixing point. So, by increasing the LFRR and decreasing the CFRR it was possible to decrease the position of the mixing point along the channel.
- Shown the effect of changing viscosity on the mixing point. Viscosity affects the lateral solution profile. For the same flow condition, the higher the viscosity of lateral solution, the higher F_{mix} value is obtained along the channel.
- Shown that by increasing LFRR and decreasing the CFRR the coagulation starting position changes by evaluating the generated clots in chip by fluorescence image analysis.
- Demonstrated by confocal studies that flow rates had no effect on clot size and shape. The obtained blood clots present fibrin fibers arrangement parallel to channel.

8. REFERENCES AND NOTES

1. Tsao, C. W. et al. Heart Disease and Stroke Statistics—2022 Update: A Report From the American Heart Association. Circulation, **2022**, 145(8), 153-639.
2. Mosesson, M. W. Fibrinogen and fibrin structure and functions. J. Thromb. Haemost. **2005**, 3(8), 1894–1904.
3. Baig, M. U. et al. Thrombolytic Therapy - statpearls - NCBI blookshelf, StatPearls. https://www.ncbi.nlm.nih.gov/books/NBK557411/ (accessed Jan 9, 2023).
4. Rabellino, M. et al. Trombectomía mecánica en el stroke isquémico agudo con el stent Solitaire AB. Neurol. Argentina, **2014**, 6(1), 36–39.
5. Kim, J. S. tPA Helpers in the Treatment of Acute Ischemic Stroke: Are They Ready for Clinical Use? J. Stroke, **2019,** 21(2), 160–174.
6. Cheng, R. et al. Acceleration of Tissue Plasminogen Activator-Mediated Thrombolysis by Magnetically Powered Nanomotors. ACS Nano, **2014**, 8(8), 7746–7754.
7. Krebs, H. A. Chemical Composition of Blood Plasma and Serum. Annu. Rev. Biochem. **1950**, 19(1), 409–430.
8. Butenas, S. Tissue Factor Structure and Function. Scientifica. **2012**, 1–15.
9. Hanson SR, et al. Blood Coagulation and Blood - Materials Interactions. In Biomaterials Science: An Introduction to Materials: Third Edition. Elsevier Inc. **2013**, 551-557.
10. Furie, B. et al. Mechanisms of Disease Mechanisms of Thrombus Formation. N. Engl. J. Med. **2018**, 359(9), 938-49.
11. Denorme, F. et al. Procoagulant platelets: novel players in thromboinflammation. Am. J. Physiol. Physiol. **2022**, 323(4), 951–958.
12. Martinez-Bulit, P. et al. In flow-based technologies: A new paradigm for the synthesis and processing of covalent-organic frameworks. Chem. Eng. J. **2022**, 435, 135117.
13. Deville, M. O. Incompressible Newtonian Fluid Mechanics. in An Introduction to the Mechanics of Incompressible Fluids, **2022**, 1–32.
14. Nader, E. et al. Blood Rheology: Key Parameters, Impact on Blood Flow, Role in Sickle Cell Disease and Effects of Exercise. Front. Physiol. **2019**, 10.
15. Chien, S. Shear Dependence of Effective Cell Volume as a Determinant of Blood Viscosity. Science, **1970**, 168(3934), 977–979.
16. McDonald, J. C. et al. Fabrication of microfluidic systems in poly(dimethylsiloxane). Electrophoresis, **2000**, 21(1), 27–40.
17. Fernández-Costa, J. M. et al. Training-on-a-Chip: A Multi-Organ Device to Study the Effect of Muscle Exercise on Insulin Secretion in Vitro. Adv. Mater. Technol. **2022**, 2200873.
18. National Center of Biotechnology Information (2023). PubChem Compound Summary for CID 33258, Allura Red AC. https://pubchem.ncbi.nlm.nih.gov/compound/Allura-Red-AC (accessed Jan 9, 2023).
19. Ketelsen, H. et al. Adsorption of brilliant blue FCF by soils. Geoderma, **1999**, 90(1), 131–145.
20. Nasatto, P. et al. Methylcellulose, a Cellulose Derivative with Original Physical Properties and Extended Applications. Polymers. **2015**, 7(5), 777–803.
21. Lang, W. et al. Physiological HEPES Buffer Proposed as a Calibrator for pH Measurement in Human Blood. Clin Chem Lab Med. **1999**, 37(5), 563–71.

22. Schwalfenberg, G. K. The Alkaline Diet: Is There Evidence That an Alkaline pH Diet Benefits Health? J. Environ. Public Health **2012**, 1–7.
23. Guo, J. et al. Determination of Brilliant Blue FCF in food and cosmetic samples by ionic liquid independent disperse liquid–liquid micro-extraction. Anal. Methods, **2013**, 5(16), 4021.
24. Abou-Gamra, Z. M. Kinetic and Thermodynamic Study for Fenton-Like Oxidation of Amaranth Red Dye. Adv. Chem. Eng. Sci. **2014**, 4(3), 285–291.
25. Shoji, K. F. et al. Fluorometric Methods for Detection of Mitochondrial Membrane Depolarization Induced by CD95 Activation. **2017**, 1557, 49–62.
26. Wojcik, K., et al. Measurements on MIMO-FRET Nano-Networks Based on Alexa Fluor Dyes. IEEE Trans. Nanotechnol. **2015**, 14(3), 531–539.
27. Schindelin, J. et al. Fiji: an open-source platform for biological-image analysis. Nat. Methods, **2012**, 9(7), 676–682.
28. Vitello, D. J. et al. Blood Density Is Nearly Equal to Water Density: A Validation Study of the Gravimetric Method of Measuring Intraoperative Blood Loss. J. Vet. Med. **2015**, 1–4.

9. ACRONYMS

r-tPA: Recombinant tissue plasminogen activator

HEPES: Hydroxyethyl)piperazine-N'-(2-ethanesulfonic acid)

MC: Methylcellulose

PDMS: Poly(dimethylsiloxane)

LFRR: Lateral flow rate ratio

CFRR: Central flow rate ratio

TPA: Tissue plasminogen activator

TF: Tissue factor

DMSO: dimethyl sulfoxide

IBEC: Institute of Bioengineering of Catalonia

Re : Reynolds number

APPENDICES

APPENDIX 1: IMAGE EDITING

First, the videos of each section of the channel must be assembled. For this, Fiji[27] (National Institutes of Health, NIH) was used, a digital image processing program that allowed us the creation of videos from images.

Images were acquired as separated PNG images and stored in a common folder as shown in (Figure S1A). Once the folder containing the channel images at a given condition was created, the images belonging to the same section of the channel were selected and opened in Image J. Then, images were assembled following the process below *Image* > *Stacks* > *Images to Stack.* The file was saved following File > Save As > AVI in JPEG and 1 fps Frame rate. The frame rate used does not actually correspond to the fps of the experiment but to the fps of the video that will be created. This process must be carried out for all tested conditions.

To produce the final image composition, we used Shotcut (Meltytech, LLC), a video editing software. First, different video tracks need to be created to load the channel section video on each one (Figure S1B). The videos of each video track were edited following by using the filter properties of *Size, position and rotation. T*he image size was reduced to a 22 % to be able to fit all the images of the channel. In this way, an adequate measure of the videos was achieved to group them along the editing background. Once the videos were grouped to form a video of the whole channel, they were exported as Tiff image sequence*,* and then the frames per second should be changed to 8. The using *export file*, the file was saved to the specific folder in images in TIFF format.

In the folder where the Tiff images were saved, 32 images were generated. We worked exclusively using images in intervals of 8. These images were chosen to get only 4 images of the entire channel, since the video editing program is not capable of saving images with a coherent frame rate. The 4 chosen images were opened in Image J to crop them and removed excess background. Then, the images were assembled following the same process as before: *Image* > *Stacks* > *Images to Stack.* Using the rectangle icon, the channel was selected and cut to obtain

only images of the channel. The images were rotated so that the channel was completely straight for its correct analysis. The images were then saved as *Image Sequence*, in PNG format and then the destination folder was selected, in this way the images would be ready for analysis.

For its subsequent study, masks of each channel were prepared to specify the study area in MATLAB code. Two channel masks, a white background mask (WB) and a black background mask (BB), were prepared. Masks must be prepared for each experiment. One of the four images of whole channel was uploaded at a determined flow rate, then the area to be studied was selected (rectangle icon). The rectangle was painted black and the background white, thus obtaining the WB mask. To get the other mask (BB), the colours in the image were inverted. Then, each mask is saved in PNG format.

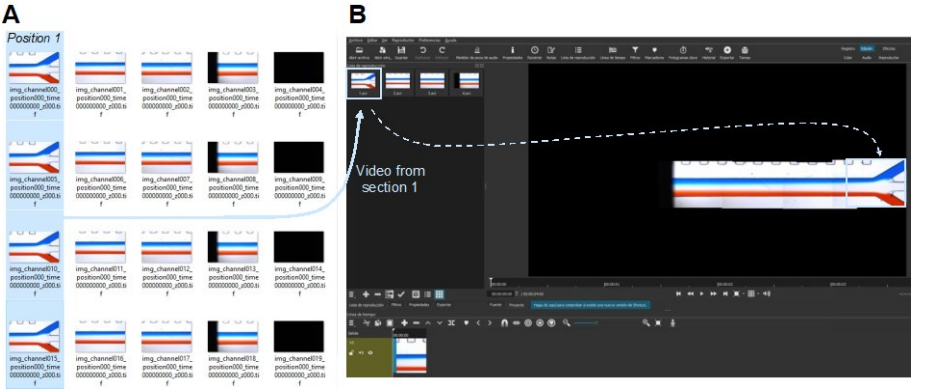

Figure S1. Pictures of (A) folder with the images taken; (B) Video editing in ShotCut

APPENDIX 2: CALCULATED Re

Lateral flow rate (µL/min)	Central flow rate (µL/min)	Total flow rate (m^3/s)	Linear velocity (m/s)	Shear rate (s^{-1})	Re Water	Re Blood
1	20	22	0.001	0.73	0.003	0.001
5	20	30	0.001	1.00	0.004	0.002
10	20	40	0.001	1.33	0.005	0.002
1	40	42	0.001	1.40	0.005	0.002
5	40	50	0.002	1.67	0.006	0.003
10	40	60	0.002	2.00	0.008	0.003
1	60	62	0.002	2.07	0.008	0.003
5	60	70	0.002	2.33	0.009	0.004
10	60	80	0.003	2.67	0.010	0.004

Table S1. Summary of Re values

APPENDIX 3: VISCOSITY MEASUREMENTS

		Viscosity at different velocity (cP)				
	Concentration (%)	**1 rpm**	**5 rpm**	**10 rpm**	**50 rpm**	**100 rpm**
Water	100	5.4	1.68	1.56	1.31	1.39
Methylcellulose	0.50	21.6	16.8	16.14	-	-
	0.25	7.2	4.2	4.02	3.80	3.82
	0.1	-	2.52	2.22	2.14	2.15
	0.05	3	2.16	1.92	1.81	1.81
	0.01	-	1.92	1.68	1.37	1.35

(a) Values of viscosity were determined using a Brookfield Ametek DVE Viscometer and a Brookfield spindle s00

Table S2. Summary of viscosity values of methylcellulose solutions and water

APPENDIX 4: FLUORESCENT IMAGE OF CHIPS

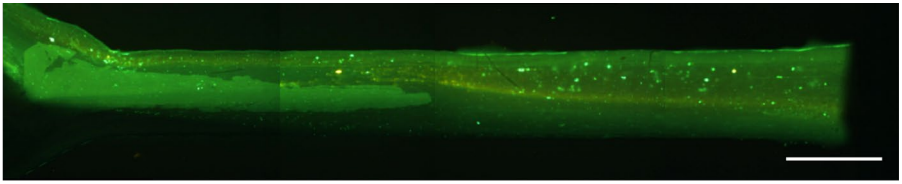

1/20/1 Chip discarded

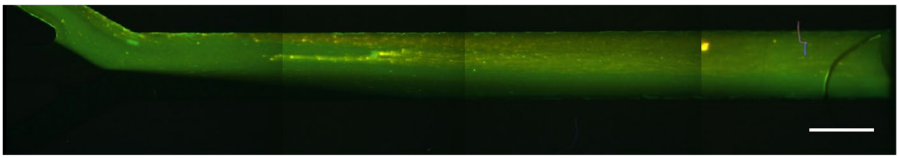

1/20/1 Chip optimized

Figure S2. Fluorescence images with chips of different geometry at 1/20/1 flow condition. Scale bar, 1 mm.

APPENDIX 5: CLOT GENERATION - CONTROL EXPERIMENTS

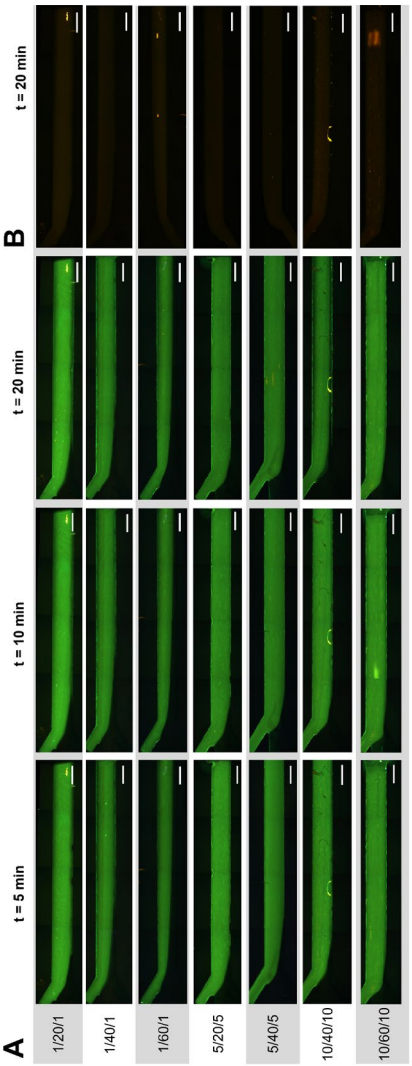

Figure S3. Fluorescent images were taken using a (A) NIKON F66-L000 ET-Triple 400/470-490/550 LED; (B) NIKON TRITC Filter Cube Set. Scale bar, 1 mm.